Variational Approach to Power Evolution in Cascaded Fiber Raman Laser

Hakan I. Tarman and Halil Berberoglu

***Abstract*—A variational approach is formulated and implemented for numerically solving a system of nonlinear two-point boundary value problem (BVP) with coupled boundary conditions modeling the power evolution in cascaded fiber Raman laser with the fiber Bragg gratings at the ends of the cavity. The nonlinearity is treated by successive linearization and the coupled boundary conditions are naturally incorporated into the system through integration in the variational setting. A global approximation of the dependent variables in terms of Legendre polynomials is used to provide a stable Lagrangian interpolation representation as well as the Legendre-Gauss quadrature for accurate numerical evaluation of integrals in the variational formulation. An initial approximate solution is constructed for the delicate convergence to the solution. The approach is validated against an approximate analytic solution and some exact integrals of the variables. The numerical experiments show exponential (spectral) accuracy achieved with much lower resolution in comparison to a widely available BVP solver. Further numerical experiments are performed to reveal the physical characteristics of the underlying model.**

***Index Terms*—Boundary-value problems, fiber Raman lasers (FRL), variational method.**

I. Introduction

FIBER RAMAN LASERs (FRLs) have attracted much attention for their many applications in optical communications. They are based on a well-known nonlinear optical process called stimulated Raman Scattering resulting in frequency down-shifted Stokes light. A typical mathematical model [1] for the power evolution is in the form of a first-order system of coupled ordinary differential equations (ODEs) of two-point boundary value problem (BVP) type. From the numerical standpoint, it is a challenging problem due to the nonlinearity and the coupled boundary conditions representing the reflected laser power at the ends of the cavity by the fiber Bragg gratings. There have been various numerical approaches to the governing BVP ranging from local approximation techniques such as shooting method [2], [3] to global approximations such as pseudospectral method [4]. A common feature of these techniques is their pointwise approach to the removal of the residual resulting from approximating the dependent variable and subsequently the differential equation. They differ, however, on the accuracy that a global method can achieve exponential (spectral) rate of convergence while a local method is only algebraically convergent.

Manuscript received April 04, 2010; revised June 12, 2010, September 03, 2010; accepted September 04, 2010. Date of publication September 16, 2010; date of current version October 27, 2010.

H. I. Tarman is with the Department of Engineering Sciences, Middle East Technical University, Ankara 06531, Turkey (e-mail: tarman@metu.edu.tr).

H. Berberoglu is with the Department of Physics, Middle East Technical University, Ankara 06531, Turkey.

Digital Object Identifier 10.1109/JLT.2010.2076774

Variational approach is a classical tool in numerically solving BVPs [5]. It is an alternative to the pointwise approach in which the differential equation is satisfied under an integral in the distributions sense. This allows flexibility in the way the residual error is minimized as well as in the incorporation of the boundary conditions into the resulting system. Furthermore, it achieves high accuracy by the use of global expansion in approximating the dependent variable and thus fewer terms are needed in the expansion to achieve this accuracy. Jacobi polynomials form convenient bases for this expansion in providing both numerically stable interpolation and highly accurate numerical integration rule via Gaussian quadrature [6]. Legendre polynomials, in particular, are computationally more efficient for variational (weak) formulation due to natural selection of unity weighting in the inner products. Selecting Legendre-Gauss-Lobatto grid points for discretization provides stable Lagrangian interpolation representation for the dependent variable as well as the quadrature points for accurate numerical evaluation of integrals. Furthermore, these points are heavily clustered near the boundaries to more accurately resolve the near-boundary behavior.

The nonlinearity of the model BVP is another challenge for the numerical treatment. It is dealt with repeated linearization of the equations around increasingly accurate intermediate solutions starting from an initial approximation in a Newton like approach. Due to the presence of a trivial solution, where the pump is depleted only by linear attenuation without generating any Stokes light, the quality of the initial approximation is crucial in steering the iterative approach towards the physical (nontrivial) solution. This is accomplished by incorporating the initial approximation technique presented in [4] to the current variational approach. Moreover, highly accurate evaluation of some integrals of the solution in the initial approximation process provides a way of assessing the degree of accuracy in the numerical results. The underlying use of Legendre polynomials and the associated Gauss quadrature provide the convenient medium for the numerical evaluation of these integrals.

II. Theoretical Model

The numerical solution procedure is developed to simulate the steady-state power evolution in a Raman gain fiber governed by the following system of coupled nonlinear ODES [1]

$$
\begin{aligned}
\pm\frac{dP_0^\pm}{dz} &= -\alpha_0 P_0^\pm - g_0 P_0^\pm (P_1^+ + P_1^-)\\
\pm\frac{dP_j^\pm}{dz} &= -\alpha_j P_j^\pm - g_j P_j^\pm (P_{j+1}^+ + P_{j+1}^-)\\
&\quad + g_j P_j^\pm (P_{j-1}^+ + P_{j-1}^-)\\
\pm\frac{dP_n^\pm}{dz} &= -\alpha_n P_n^\pm + g_n P_n^\pm (P_{n-1}^+ + P_{n-1}^-). \qquad (1)
\end{aligned}
$$

where P_0, P_j represent the pump and jth-order Stokes light for $j = 1, \ldots, n$, respectively. The $\pm$ stands for the forward/backward propagating wave in the cavity. Here, α denotes the intrinsic fiber loss coefficient and g the Raman gain between adjacent waves. The boundary conditions for the forward pumping configuration are given by the input pump power P_{in} and by the Bragg gratings that are located at point $z = 0$ and $z = L$

$$\begin{aligned} &P_0^+(0) = P_{\text{in}}, \quad P_i^-(L) = R_i^+ P_i^+(L), \\ &P_j^+(0) = R_j^- P_j^-(0) \end{aligned} \tag{2}$$

for $i = 0, \ldots, n$ and $j = 1, \ldots, n$. where R is the reflectivity coefficients of Bragg gratings with the superscripts $\pm$ denoting the output side ($z = L$) and the input side ($z = 0$), respectively. $R_n^+ = R_{\text{OC}}$ is the reflectivity of coefficient of the output coupler. L is the length of the fiber cavity. The amplified spontaneous emission effect and Rayleigh backscattering are not included.

III. Variational Formulation

It is convenient to work with the linearized form of the model BVP (1) by introducing the increment function $h_j^\pm$ that satisfies

$$\begin{aligned} &\pm \frac{dh_0^\pm}{dz} + \alpha_0 h_0^\pm + g_0 h_0^\pm (P_1^+ + P_1^-) + g_0 P_0^\pm (h_1^+ + h_1^-) \\ &\quad = F_0^\pm (P_0^\pm, P_1^\pm), \\ &\qquad \pm \frac{dh_j^\pm}{dz} + \alpha_j h_j^\pm + g_j h_j^\pm (P_{j+1}^+ + P_{j+1}^- - P_{j-1}^+ - P_{j-1}^-) \\ &\qquad + g_j P_j^\pm (h_{j+1}^+ + h_{j+1}^- - h_{j-1}^+ - h_{j-1}^-) \\ &\quad = F_j^\pm (P_{j-1}^\pm, P_j^\pm, P_{j+1}^\pm), \\ &\qquad \pm \frac{dh_n^\pm}{dz} + \alpha_n h_n^\pm - g_n h_n^\pm (P_{n-1}^+ + P_{n-1}^-) \\ &\qquad - g_n P_n^\pm (h_{n-1}^+ + h_{n-1}^-) = F_n^\pm (P_{n-1}^\pm, P_n^\pm) \end{aligned} \tag{3}$$

for $j = 1, \ldots, n-1$, together with

$$h_0^+(0) = 0 \quad h_i^-(L) = R_i^+ h_i^+(L) \quad h_j^+(0) = R_j^- h_j^-(0) \tag{4}$$

for $i = 0, \ldots, n$ and for $j = 1, \ldots, n$. This is obtained by substituting $P_j^\pm + h_j^\pm$ into the model BVP (1) and collecting the terms containing only the known approximate solution $P_j^\pm$ in $F_j^\pm$. Repeated application of this procedure leads to the Newton iteration.

The solution to the linearized system is sought in the subspace of functions

$$V = \{ v_j^\pm \in H[0, L] \,|\, v_0^+(0) = 0, \quad j = 0, \ldots, n \} \tag{5}$$

in an Hilbert space $H[0, L]$ endowed with an inner product

$$\langle f, g \rangle = \int_0^L f(z) g(z) dz. \tag{6}$$

The system (3) is then projected onto the subspace V using Galerkin procedure to get the variational (weak) form of the equations

$$\begin{aligned} &\pm \left[h_0^\pm w_0^\pm \right]_0^L \mp \left\langle h_0^\pm, \frac{dw_0^\pm}{dz} \right\rangle + \alpha_0 \langle h_0^\pm, w_0^\pm \rangle \\ &+ g_0 \left\langle h_0^\pm (P_1^+ + P_1^-), w_0^\pm \right\rangle + g_0 \langle P_0^\pm (h_1^+ + h_1^-), w_0^\pm \rangle \\ &\quad = \langle F_0^\pm, w_0^\pm \rangle, \\ &\pm [h_j^\pm w_j^\pm]_0^L \mp \left\langle h_j^\pm, \frac{dw_j^\pm}{dz} \right\rangle + \alpha_j \langle h_j^\pm, w_j^\pm \rangle \\ &+ g_j \langle h_j^\pm (P_{j+1}^+ + P_{j+1}^- - P_{j-1}^+ - P_{j-1}^-), w_j^\pm \rangle \\ &+ g_j \langle P_j^\pm (h_{j+1}^+ + h_{j+1}^- - h_{j-1}^+ - h_{j-1}^-), w_j^\pm \rangle \\ &\quad = \langle F_j^\pm, w_j^\pm \rangle, \\ &\pm [h_n^\pm w_n^\pm]_0^L \mp \left\langle h_n^\pm, \frac{dw_n^\pm}{dz} \right\rangle + \alpha_n \left\langle h_n^\pm, w_n^\pm \right\rangle \\ &- g_n \langle h_n^\pm (P_{n-1}^+ + P_{n-1}^-), w_n^\pm \rangle \\ &- g_n \langle P_n^\pm (h_{n-1}^+ + h_{n-1}^-), w_n^\pm \rangle \\ &\quad = \langle F_n^\pm, w_n^\pm \rangle \end{aligned} \tag{7}$$

after integrating by parts. Here, $h, w \in V$ are referred to as trial and test functions, respectively. The procedure allows natural inclusion of the boundary conditions (4) in the variational form by expanding the brackets and using (4) as follows

$$\begin{aligned} &[h_0^+ w_0^+]_0^L = h_0^+(L) w_0^+(L) \\ &[h_i^- w_i^-]_0^L = R_i^+ h_i^+(L) w_i^-(L) - h_i^-(0) w_i^-(0) \\ &[h_j^+ w_j^+]_0^L = h_j^+(L) w_j^+(L) - R_j^- h_j^-(0) w_j^+(0) \end{aligned} \tag{8}$$

for $i = 0, \ldots, n$ and $j = 1, \ldots, n$.

IV. Approximation Procedure

The subspace of functions V is approximated by using orthogonal polynomials, namely, Legendre polynomials. They are computationally efficient for variational formulation due to the natural selection of unity weighting in the inner products and availability of highly accurate Gauss-Lobatto-Legendre quadrature to evaluate the inner product integrals. They can be approximated by

$$\langle f, g \rangle = \int_0^L f(z) g(z) dz \approx \frac{L}{2} \sum_{q=0}^{m} \omega_q f(z_q) g(z_q) \tag{9}$$

which is exact for the integrand being a polynomial of order $2m - 1$ or less. Here, ω_q are the quadrature weights and $z_q = z(x_q)$ are the image of the quadrature nodes x_q under the map $z(x) = (L/2)(x + 1)$ from the natural (reference) interval $[-1, 1]$ to the computational interval $[0, L]$. The approximation procedure is completed with a finite nodal expansion

$$h_j^\pm(z(x)) = \sum_{p=0}^{m} h_{j,p}^\pm L_p(x) \tag{10}$$

in terms of Legendre-Lagrangian interpolants $L_p(x)$ satisfying the cardinality property $L_p(x_q) = \delta_{pq}$ where $h_j(z_p) = h_{j,p}$.

The homogeneous condition $h_0^+(0) = 0$ is satisfied by restricting the index range to $0 < p \leq m$ in the expansion for h_0^+ where $z_0 = 0$ is assumed.

The expansion (10) is substituted into (7) resulting in a system of linear equations

$$\begin{aligned}
&\pm [h_0^{\pm} L_s]_{-1}^{+1} \mp \sum_{q=0}^{m} \omega_q h_{0,q}^{\pm} L'_{s,q} + \frac{L}{2}\omega_s h_{0,s}^{\pm}(\alpha_0 \\
&+ g_0(P_{1,s}^+ + P_{1,s}^-)) + \frac{L}{2} g_0 \omega_s P_{0,s}^{\pm}(h_{1,s}^+ + h_{1,s}^-) \\
&\quad = \frac{L}{2}\omega_s F_{0,s}^{\pm}, \\
&\pm [h_j^{\pm} L_s]_{-1}^{+1} \mp \sum_{q=0}^{m} \omega_q h_{j,q}^{\pm} L'_{s,q} + \frac{L}{2}\omega_s h_{j,s}^{\pm}(\alpha_j \\
&+ g_j(P_{j+1,s}^+ + P_{j+1,s}^- - P_{j-1,s}^+ - P_{j-1,s}^-)) \\
&+ \frac{L}{2} g_j \omega_s P_{j,s}^{\pm}(h_{j+1,s}^+ + h_{j+1,s}^- - h_{j-1,s}^+ - h_{j-1,s}^-) \\
&\quad = \frac{L}{2}\omega_s F_{j,s}^{\pm}, \\
&\pm \left[h_n^{\pm} L_s\right]_{-1}^{+1} \mp \sum_{q=0}^{m} \omega_q h_{n,q}^{\pm} L'_{s,q} + \frac{L}{2}\omega_s h_{n,s}^{\pm}(\alpha_n \\
&- g_n(P_{n-1,s}^+ + P_{n-1,s}^-)) \\
&- \frac{L}{2} g_n \omega_s P_{n,s}^{\pm}(h_{n-1,s}^+ + h_{n-1,s}^-) \\
&\quad = \frac{L}{2}\omega_s F_{n,s}^{\pm}
\end{aligned} \tag{11}$$

for as many unknown nodal values $h_{j,s}^{\pm}$ after selecting $w = L_s(x)$ for $s = 0, \ldots, m$ except for the equation involving h_0^+ where the index is restricted to $s = 1, \ldots, m$ due to the consideration of the homogeneous condition. The brackets similarly follow

$$\begin{aligned}
[h_0^+ L_s]_{-1}^{+1} &= h_{0,m}^+ \delta_{sm} \\
[h_i^- L_s]_{-1}^{+1} &= R_i^+ h_{i,m}^+ \delta_{sm} - h_{i,0}^- \delta_{s0} \\
[h_j^+ L_s]_{-1}^{+1} &= h_{j,m}^+ \delta_{sm} - R_j^- h_{j,0}^- \delta_{s0}
\end{aligned} \tag{12}$$

for $i = 0, \ldots, n$ and for $j = 1, \ldots, n$ with δ_{ij} the Kronecker symbol. The system (11)–(12) can be cast into matrix form

$$\begin{aligned}
-\{H_j\}\mathbf{WD} + \{\delta_{j0}\mathbf{R}_j^- H_j\} + \{\delta_{im}\mathbf{R}_i^+ H_i\} \\
-\frac{L}{2}\{\omega_j \mathbf{J}_j H_j\} = \{F_j\}\mathbf{W}
\end{aligned} \tag{13}$$

with $\{F_j\} = -\{P_j\}\mathbf{D}^\top + (L/2)\{G_j\}$ where the nodal values are arranged as

$$H_j = [h_{0,j}^+ \quad h_{0,j}^- \quad \cdots \quad h_{n,j}^-]^\top \tag{14}$$
$$\{H_j\} = [H_0 \quad H_1 \quad \cdots \quad H_m] \tag{15}$$

and similarly for $\{P_j\}$. Furthermore, $D_{ij} = L'_j(x_i)$ is the differentiation matrix

$$\mathbf{W} = \mathrm{diag}([\omega_0 \quad \omega_1 \quad \cdots \quad \omega_m]) = \begin{bmatrix} \omega_0 & & & \\ & \omega_1 & & \\ & & \ddots & \\ & & & \omega_m \end{bmatrix}, \tag{16}$$

$$\mathbf{J}_j = \mathbf{A} + \mathrm{diag}(\mathbf{B}P_j) + \mathrm{diag}(P_j)\mathbf{B}, \tag{17}$$
$$G_j = \mathbf{A}P_j + \mathrm{diag}(\mathbf{B}P_j)P_j. \tag{18}$$

The data of the problem are collected in the block form by

$$\mathbf{A} = \mathrm{blkdiag}(\mathbf{A}_j) = \begin{bmatrix} \mathbf{A}_0 & & & \\ & \mathbf{A}_1 & & \\ & & \ddots & \\ & & & \mathbf{A}_n \end{bmatrix} \tag{19}$$

$$\mathbf{B} = \begin{bmatrix} \mathbf{0} & \mathbf{B}_0^+ & & \\ \mathbf{B}_1^- & \mathbf{0} & \ddots & \\ & \ddots & \ddots & \mathbf{B}_{n-1}^+ \\ & & \mathbf{B}_n^- & \mathbf{0} \end{bmatrix} \tag{20}$$

with

$$\mathbf{A}_j = \begin{bmatrix} -\alpha_j & 0 \\ 0 & \alpha_j \end{bmatrix}, \quad \mathbf{B}_j^{\pm} = \pm g_j \begin{bmatrix} -1 & -1 \\ 1 & 1 \end{bmatrix} \tag{21}$$

and the boundary data $\mathbf{R}^{\pm} = \mathrm{blkdiag}(\mathbf{R}_k^{\pm})$ with

$$\mathbf{R}_i^+ = \begin{bmatrix} 1 & 0 \\ R_i^+ & 0 \end{bmatrix}, \quad \mathbf{R}_j^- = \begin{bmatrix} 0 & -R_j^- \\ 0 & -1 \end{bmatrix} \tag{22}$$

for $i = 0, \ldots, n$ and for $j = 1, \ldots, n$ with

$$\mathbf{R}_0^- = \begin{bmatrix} -1 & 0 \\ 0 & -1 \end{bmatrix}. \tag{23}$$

Further rearrangement of (13) gives the linear system

$$\begin{aligned}
\mathbf{Q}[-(\mathbf{D}^\top\mathbf{W}) \otimes \mathbf{I}_N + \mathbf{Bc} - \mathrm{blkdiag}(\omega_j \mathbf{J}_j)]\mathbf{Q}^\top H \\
= \mathbf{Q}\,\mathrm{vec}\,(\{F_j\}\mathbf{W})
\end{aligned} \tag{24}$$

for the direct evaluation of the restricted (unknown) nodal values $H = \mathbf{Q}\,\mathrm{vec}(\{H_j\})$ where

$$\mathrm{vec}(\{H_j\}) = [\mathbf{H}_0^\top \quad \mathbf{H}_1^\top \quad \cdots \quad \mathbf{H}_m^\top]^\top \tag{25}$$

$$\mathbf{Bc} = \begin{bmatrix} \mathbf{R}^- & & \\ & \mathbf{0} & \\ & & \mathbf{R}^+ \end{bmatrix} \tag{26}$$

$\mathbf{I}_N$ is the $N \times N$ identity matrix with $N = 2n + 2$, $\otimes$ is the Kronecker product [7] and $\mathbf{Q}$ is the Boolean restriction matrix [8] comprising columns of the identity matrix with a column of

TABLE I
SIMULATION PARAMETERS [1]

Stokes order	Frequency (THz)	Raman Gain (1/W/km)	Absorption (km^{-1})
0(pump)	281	2.576	0.143
1	268	2.455	0.118
2	255	2.114	0.0969
3	242	1.786	0.0852
4	228	1.474	0.0814
5	215	1.181	0.194
6	202	0.912	0.0436

zeros at the location corresponding to nodal point $z_0 = 0$ at which $h_0^+(0) = 0$.

V. NUMERICAL IMPLEMENTATION

For the numerical experiments, the simulation parameters used in [1] corresponding to a sixth-order $(n = 6)$ cascaded Raman fiber laser with silica-based fiber are considered as listed in Table I. In order to stay clear of the trivial solution, namely

$$P_0^+(z) = P_{\text{in}} \exp(-\alpha_0 z)$$
$$P_0^-(z) = R_0^+ P_{\text{in}} \exp(-\alpha_0(z - 2L)) \quad (27)$$

and $P_j^{\pm} = 0$ for $j \geq 1$, the initial approximation should carry as much property of the actual (nontrivial) solution as possible. Such an approximation is already constructed in [4] based on the observation that the system (1) allows the exact evaluation of some integrals of the solution. The construction procedure is summarized below for the particular case of $n = 6$ for clarity and completeness.

Assuming $P_j^{\pm} > 0$ and integrating the coupled system (1) from 0 to L result in the following system of equations

$$U_0^+ = -\alpha_0 - g_0 S_1 \quad (28)$$

$$\begin{bmatrix} g_2 & -g_2 & 0 \\ 0 & g_4 & -g_4 \\ 0 & 0 & g_6 \end{bmatrix} \begin{bmatrix} S_1 \\ S_3 \\ S_5 \end{bmatrix} = \begin{bmatrix} U_2^+ + \alpha_2 \\ U_4^+ + \alpha_4 \\ U_6^+ + \alpha_6 \end{bmatrix} \quad (29)$$

$$\begin{bmatrix} -g_1 & 0 & 0 \\ g_3 & -g_3 & 0 \\ 0 & g_5 & -g_5 \end{bmatrix} \begin{bmatrix} S_2 \\ S_4 \\ S_6 \end{bmatrix} = \begin{bmatrix} U_1^+ + \alpha_1 - g_0 S_0 \\ U_3^+ + \alpha_3 \\ U_5^+ + \alpha_5 \end{bmatrix} \quad (30)$$

where

$$S_j = \frac{1}{L} \int_0^L (P_j^+ + P_j^-) dz \quad (31)$$

and

$$U_j^+ = \frac{1}{L} \ln(P_j^+(L)/P_j^+(0)) \quad (32)$$

with $U_j^+ = -(1)/(2L) \ln(R_j^+ R_j^-), j \geq 1$. These quantities can be used to construct an approximate solution in the assumed exponential form

$$P_j^{\pm}(z) = P_j^{\pm}(0) \exp(\pm\beta_j z) \quad (33)$$

whose parameters can be obtained by using $\beta_j = -U_j^+$ and

$$P_j^+(0) = \frac{-S_j U_j^+ L}{(1 - \exp(U_j^+ L))(1 + R_j^+ \exp(U_j^+ L))} \quad (34)$$

$$P_j^-(0) = P_j^+(0) R_j^+ \exp(2U_j^+ L) \quad (35)$$

with $P_0^+(0) = P_{\text{in}}$. A construction algorithm is then follows.

1) Solve (29) for the values of S_1, S_3, S_5.
2) Solve (28) for U_0^+.
3) Solve (34) for S_0 using $U_0^+, P_0^+(0) = P_{\text{in}}$.
4) Solve (30) for $S_2, S_4 S_6$.

Finally, the approximate solution (33) can be constructed using the computed values and (34)–(35). Starting from the constructed initial approximation, the solution strategy consists of iterating the variational solution procedure until $\|h\|_\infty$ attains its smallest value and stagnates. The attenable accuracy for given m is restricted due to the fact that the solution is searched within the polynomial space of degree $\leq m$. At that point, the accuracy in the solution is assessed by comparing $\mathbf{S_0}= [S_1 S_3 S_5]$ against $\tilde{\mathbf{S}}_\mathbf{0}= [\tilde{S}_1 \tilde{S}_3 \tilde{S}_5]$ in the maximum norm $\|\mathbf{S_0} - \tilde{\mathbf{S}}_\mathbf{0}\|_\infty$ where

$$\tilde{S}_j = \frac{1}{2} \sum_{q=0}^{m} \omega_q (P_j^+(z_q) + P_j^-(z_q)). \quad (36)$$

We have solved the model system (1) using the proposed algorithm for the case with 96.7% reflectivity mirrors and 10% output mirror. The cavity length is taken as 150 m and the injected pump power 6 W. The resulting computed wave power profiles (curves) are shown in Fig. 1 in comparison to the analytic solution (symbols) that is also presented in Fig. 2 of [1] for the same parameter values. The comparison yields a relative error of around 1% of the computed solution at the resolution $m = 14$. The wave patterns are typical as pointed out in [9] in that the two Stokes light adjacent to the pump and the 5th Stokes lights are of fundamental standing wave type.

The resulting variation of the error $\|\mathbf{S_0} - \tilde{\mathbf{S}}_\mathbf{0}\|_\infty$ with m is shown in Fig. 2. The runs take typically 3–4 successive iterations until the attainable accuracy is obtained for given m. The efficiency of the solution technique in achieving high accuracy for very low values of the resolution m is shown. The exponential accuracy is clearly visible in the decay trend of the error curve. This should be compared with the error values resulting from the use of the computed solution obtained by employing a widely available BVP solver [10]. It should be noted that the

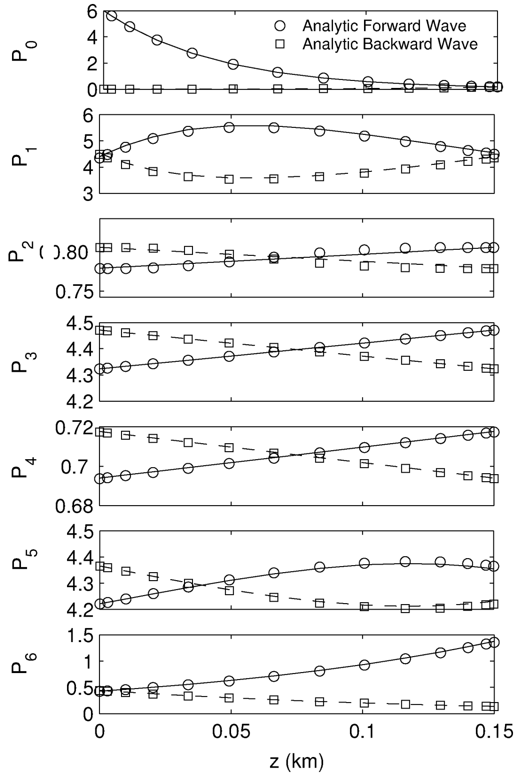

Fig. 1. Computed Stokes powers inside the cavity obtained using a resolution $m = 14$ in comparison to the approximate analytic solution [1].

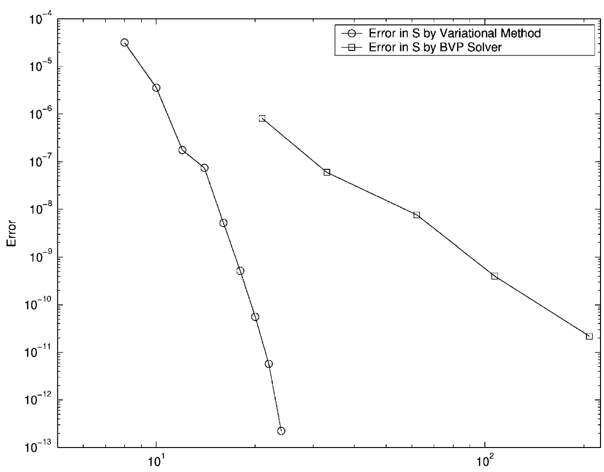

Fig. 2. Variation of the error $\|\mathbf{S_0} - \tilde{\mathbf{S}}_\mathbf{0}\|_\infty$ with the resolution m. The high resolving power of the underlying Legendre polynomials for given m and the exponential decay trend of the curve are visible in comparison to the algebraic convergence in the case of the BVP solver [10].

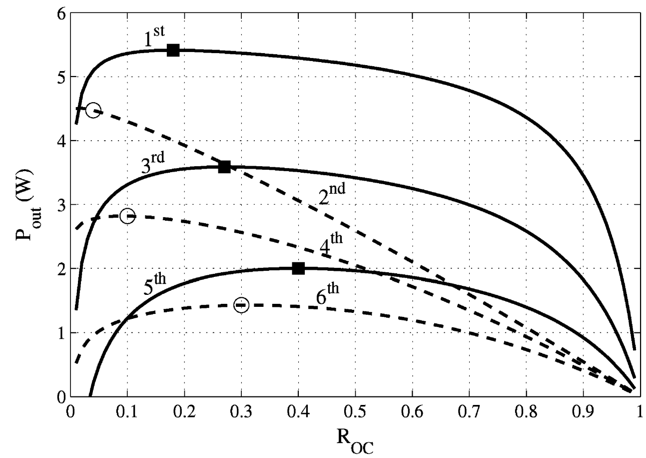

Fig. 3. Oputput power versus reflectivity of OC for each Stokes-order. Solid curves correspond to the odd number and dash curves to the even number of Stokes waves in the cavity. Markers on each curve point to the optimum values of $\mathrm{R_{OC}}$ for the input pump power of 6 W. See Table II.

TABLE II
SIMULATION RESULTS

Stokes order	Optimum R_{OC}	Threshold Power (W)	Efficiency (%)
1	0.18	1.3	94
2	0.04	0.4	78
3	0.27	1.5	67
4	0.10	0.8	53
5	0.40	2	42
6	0.30	1.6	31

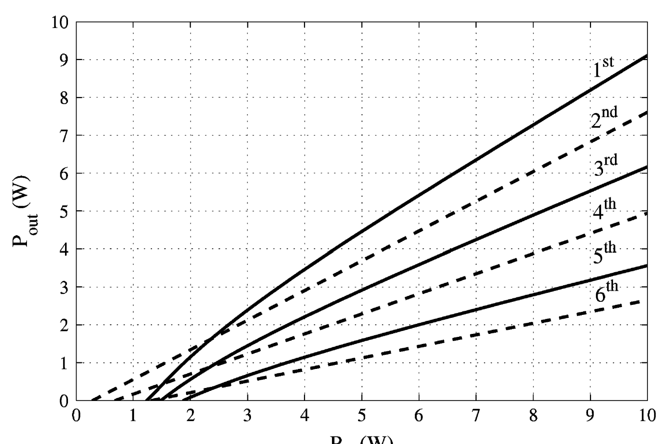

Fig. 4. Input pump power versus the output pump powers for each Stokes-order. Solid and dash curves represent the odd and even number of Stokes waves, respectively. The threshold and efficiency values are listed in Table II.

numerical experiments show that the BVP solver fails to produce correct solution unless the current initial approximation is provided. The solver is based on local polynomial approximation and can only achieve algebraic speed of convergence as it is clear in Fig. 2 in comparison.

In order to complete the discussion, some numerical experiments are performed on the design parameters (Table I). In the present analysis, the fiber length and intermediate Bragg reflectivities are fixed at 150 m. and 96.7%, respectively. The input power of 6 W is injected from the input end of the cavity. In Fig. 3, the output power is shown against the reflectivity of output coupler (OC) for each Stokes-order separately. Each curve in Fig. 3 is obtained by successively adding Stokes-orders into the designed cavity. For instance, second-order Stokes means that our fiber cavity consists of only the first and the second Stokes-orders. The square and circle markers on the curves in Fig. 3 point to the optimum OC reflectivity for the specified Stokes-orders. These optimum values minimizes the residual pump power at $z = 0$. It clearly shows that even- and odd-orders are interrelated and behave differently as pointed out in [11] for the undepleted pump case. As the Stokes-order gets higher for the given fixed input pump power, the optimum OC reflectivity values gets higher as indicated by the markers on each curve sliding to the right. It also shows that lower (higher) OC reflectivity minimizes the residual pump power when Stokes-order is even (odd) in agreement with [1]. It is observed that as the input pump power is increased starting from the corresponding threshold values for each Stokes-order, the optimum OC values shift to the left towards lower values.

The optimum OC values from Fig. 3 are then used in Fig. 4, which shows the corresponding output pump powers against the input powers for each Stokes-order in the cavity. The threshold and efficiency values are listed in Table II. The efficiency values gradually decrease as more Stokes-orders are added into the cavity. They satisfy the maximum achievable slope efficiency value g_n/g_0 stated in [11], where n is the Stokes-order considered. For instance, the slope efficiency for a fifth Stokes-order can not exceed 46% $(= 1.181 \div 2.576)$ which completely agrees with our simulation results of 42%.

VI. Conclusion

The accuracy and the robustness of the approach has been tested in the numerical experiments involving various parameter values. Variational approach with the successive linearization underlying Newton method is demonstrated to be a natural tool in treating the nonlinearity and the coupled boundary conditions forming the most challenging features of the model BVP governing the power evolution in FRLs. The use of the Legendre polynomials as the approximation medium avails the numerically stable interpolation property, high resolving power and the highly accurate Gaussian quadrature for numerical integration. The quadrature points as roots to Legendre polynomials and the quadrature weights are not known in closed form and must be computed numerically. However, various routines are available in literature for this purpose and more [12].

References

[1] B. Burgoyne, N. Godbout, and S. Lacroix, "Theoretical analysis of nth-order cascaded continuous-wave Raman fiber lasers. I. Model and resolution," *J. Opt. Soc. Amer. B*, vol. 22, no. 4, pp. 764–771, Apr. 2005.

[2] F. Leplingard, C. Martinelli, S. Borne, L. Lorcy, D. Bayart, F. Castella, P. Chartier, and E. Faou, "Modelling of multiwavelength Raman fiber lasers using a new and fast algorithm," *IEEE Photon. Technol. Lett.*, vol. 16, no. 12, pp. 2601–2603, Dec. 2004.

[3] H. Kaidi, Z. Xiaojun, Q. Zujun, W. Haocheng, and Z. Zili, "A novel fast numerical algorithm for cascaded Raman fiber laser using the analytic approximate solution," *Opt. Commun.*, vol. 271, pp. 257–262, 2007.

[4] H. Tarman and H. Berberoglu, "Efficient numerical algorithm for cascaded Raman fiber lasers using a spectral method," *J. Lightw. Technol.*, vol. 27, no. 13, p. 2289, Jul. 2009.

[5] O. Axelsson and V. A. Barker, *Finite Element Solution of Boundary Value Problems: Theory and Computation*. Philadelphia, PA: SIAM, 2001.

[6] J. S. Hesthaven, S. Gottlieb, and D. Gottlieb, *Spectral Methods for Time-Dependent Problems*. Cambridge, U.K.: Cambridge Univ. Press, 2007.

[7] A. Graham, *Kronecker Products and Matrix Calculus With Applications*. Chichester, U,K.: Ellis Horwood Ltd., 1981.

[8] M. O. Deville, P. F. Fischer, and E. H. Mund, *High-Order Methods for Incompressible Fluid Flow*. Cambridge, U.K.: Cambridge Univ. Press, 2002.

[9] S. D. Jackson and P. H. Muir, "Theory and numerical simulation of nth-order cascaded Raman fiber lasers," *J. Opt. Soc. Amer. B*, vol. 18, no. 9, pp. 1297–1305, Sep. 2001.

[10] L. F. Shampine, M. W. Reichelt, and J. Kierzenka, Solving BVPs for Ordinary Differential Equations in Matlab with bvp4c [Online]. Available: http://www.mathworks.com/bvp_tutorial [Online]. Available:

[11] B. Burgoyne, N. Godbout, and S. Lacroix, "Theoretical analysis of nth-order cascaded continuous-wave Raman fiber lasers. II. Optimization and design rules," *J. Opt. Soc. Amer. B*, vol. 22, no. 4, pp. 772–776, Apr. 2005.

[12] J. A. C. Weideman and S. C. Reddy, "A Matlab differentiation matrix suite," *ACM Trans. Math. Sotw.*, vol. 26, pp. 465–519, 2000.

Hakan I. Tarman was born in Izmir, Turkey. He received the B.S. degrees both in mechanical engineering and mathematics, the M.S. degree in mechanical engineering, and the Ph.D. degree in applied mathematics from Brown University, Providence, Rhode Island, USA, in 1982, 1984, and 1989, respectively.

He is currently a Professor at the Engineering Sciences Department, Middle East Technical University, Ankara, Turkey. His research interests include spectral methods and computational mechanics.

Halil Berberoglu was born in Denizli, Turkey. He received the B.S. degree in engineering physics, the M.S. degree in physics from Lehigh University, Bethlehem, PA, USA, and the Ph.D. degree in physics from Middle East Technical University (METU), Ankara, Turkey, in 1992, 1996, and 2007, respectively.

He is currently a research associate at METU. His research interests include fiber Raman lasers, amplifiers, and Terahertz Time-Domain Spectroscopy.